Eur. Phys. J. Appl. Phys. (2015) 70: 10403
DOI: 10.1051/epjap/2015150019

THE EUROPEAN PHYSICAL JOURNAL APPLIED PHYSICS

Regular Article

Investigation of physical properties of screen printed nanosized ZnO films for optoelectronic applications

Rayees Ahmad Zargar[1,a], Manju Arora[2], and Aurangzeb Khurram Hafiz[1]

[1] Department of Physics, Jamia Millia Islamia, New Delhi 110025, India
[2] CSIR-National Physical Laboratory, Dr. K.S. Krishnan Marg, New Delhi 110012, India

Received: 12 January 2015 / Received in final form: 21 March 2015 / Accepted: 25 March 2015
Published online: 24 April 2015 –

Abstract. Nanosized ZnO particles derived from chemical co-precipitation route were used for casting ZnO films by screen printing method followed by sintering at two different temperatures. The variation in structural, optical and electrical properties of these films with temperature have been investigated by XRD, SEM, FTIR, Raman, UV-VIS, EPR and four probe analytical techniques. XRD patterns of these films exhibit polycrystalline nature with hexagonal wurtzite structure and SEM images reveal the smooth, dense and without any cracks/damage porous surface morphology. Infrared transmission spectra shows peaks pertaining to Zn-O stretching modes and their multiphonon modes. While Raman spectra exhibited strong peaks of E_2 (high) phonon and overtone of surface phonon mode at 429 cm^{-1} and 1144 cm^{-1} respectively with weak components of LO and TO branches. The direct band gap energy of these films showed narrowing of band gap from 3.21 eV to 3.12 eV on increasing sintering temperature from 500 °C to 600 °C. DC conductivity measurements confirmed semiconducting behaviour and showed lowering of activation energy. EPR spectra showed single narrow line resonance signal of g-value $\sim$ 1.9469 due to oxygen vacancies which are produced during synthesis of ZnO nanoparticles by sol-gel process. These studies revealed that on increasing sintering temperature the crystallinity of the film improves with reduction in lattice deformations in these screen printed ZnO films.

1 Introduction

The most important characteristics of the material in the nanosize regime are their ability to change their physical properties due to large surface to volume ratio. In 1980s, a considerable progress was achieved in the field of material science to understand the size related properties of the materials [1]. ZnO is II–VI semiconductor compound with tuneable wide band gap energy of ∼3.4 eV and a large exciton binding energy of 60 meV at room temperature [2]. Nanocrystalline ZnO exhibits variety of morphological structures like nanorods, nanowires, nanoribbon, nanoflower, nanowalls, quantum dots, nanopyramids, etc. [3–8]. It exhibits a prolific combination of multifunctional properties especially structural, thermal, semiconducting, optoelectronic, optical and piezoelectric properties. Because of such remarkable properties, it is one of the most extensively studied material of past decade. ZnO finds lots of applications in the field of electronic, optoelectronic devices, sensor, biomedical, energy, environment, etc. [9–12].

The thin and thick films of ZnO are deposited by various techniques such as chemical vapour deposition, spray pyrolysis, molecular beam epitaxy, spin coating, dip coating, chemical bath deposition, screen printing, hydrothermal and solvothermal, etc. [13–18]. Screen printing, an eco-friendly, economic, suitable for large area deposition technique has been generally used by industries for rapid deposition of thick films over large areas [18–20]. Its well defining aspect regarding the deposition in concerned areas of substrate allows its maximum utility in electronic devices.

The aim of present work deals with preparation procedure of nanosized ZnO films by screen printing technique and studies the variation in their structural, optical and electrical properties with respect to increase in sintering temperature.

2 Experimental measurements

Zinc sulphate heptahydrate and sodium hydroxide solution were mixed slowly dropwise in molar ratio of 1:2 under vigorous stirring and after mixing, the stirring was continued further for 12 h. The obtained precipitate was filtered and washed thoroughly with deionised water. Then dried in oven at 100 °C and ground to fine powder using fine agate mortar [21]. The paste was prepared by thoroughly

[a] e-mail: rayeesphy12@gmail.com

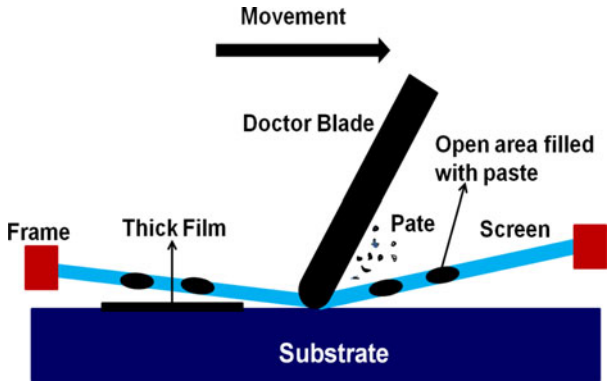

Fig. 1. Schematic diagram of screen printing technique.

mixing extracted ZnO powder with anhydrous $ZnCl_2$ used as an adhesive agent and ethylene glycol as a binder. The prepared paste was screen printed on glass substrates which were pre-cleaned with acetone and deionised water and kept in oven at 60 °C for 10 min. The as-deposited films were dried at 110 °C for 2 h in order to reduce the solvent partially and for porosity of the film [22]. The films were further annealed in a muffle furnace in an open atmosphere at 500 °C and 600 °C for 10 min so as to obtain the desired ZnO film and removal of organic materials [23]. The films are approximately 1 μm thick. The schematic of screen printing process used for deposition of ZnO film is presented in Figure 1. During deposition process, the screen is placed a few millimetres above the surface of the substrate and the paste is dispersed through squeeze (doctor blade) [24]. In this way ZnO film is produced.

X-ray diffraction pattern was recorded on advanced Rigaku diffractometer in the 2θ range of 20°–75° using Cu-Kα X-ray radiation source. Taylor Hobson (Taly step, UK) instrument was used for film thickness measurement. The surface morphological information was derived by using scanning electron microscope (SEM, LEO-440, UK). Raman spectrum was recorded using a Horiba Jobin Yvon laser spectrometer 6400. IR transmission spectra were recorded by Shimadzu-8400S, Japan spectrophotometer in the range 2000–550 cm^{-1} at ambient temperature with 4 cm^{-1} resolution. The optical absorption spectrum was recorded by Hitachi spectrometer-3900 in the 250–1000 nm range. DC conductivity measurement was done by using standard four probe technique. EPR spectra were recorded on X-band, Varian Make, E112 EPR spectrometer in 3300 G ± 2000 G region at 10 mW microwave power, 9.36 GHz microwave frequency and 100 kHz modulation frequency. 1,1 diphenyl 2-picryl hydrazyl (DPPH) was used as standard reference material for the calibration of instrument and evaluation of spin concentration.

3 Results and discussions

3.1 Structural analysis

To confirm the formation, purity and phase crystallinity of the sintered samples was examined using powder X-ray diffractometer. The sharp intense peaks of ZnO films show the polycrystalline nature with preferential orientation along (1 0 1) plane without any impurity peaks, suggesting the single phase formation of ZnO. The diffraction peaks observed in XRD patterns of ZnO films sintered at 500 °C and 600 °C are indexed as shown in the Figure 2.

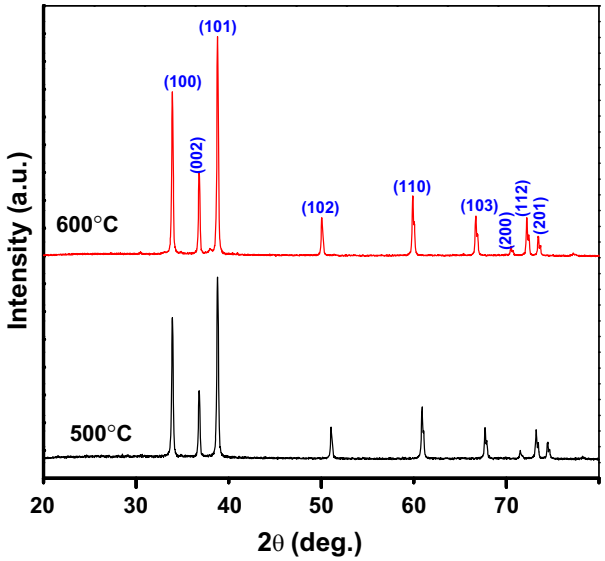

Fig. 2. XRD pattern of nanosized ZnO thick films sintered at different temperatures.

The average crystallite size was calculated by using Debye-Scherrer's formula [25] from the most intense (1 0 1) diffraction in both the samples. It has been found increase with increasing substrate temperature and the values are very close to the earlier reported result [26].

$$D = \frac{0.9\lambda}{\beta \cos\theta}, \tag{1}$$

where D is the grain boundary size (in nm), λ is the X-ray wavelength β is the width (in radians) at half the maximum peak intensity and θ is the Bragg angle. These parameters are listed in Table 1.

3.2 Surface morphological analysis

Figure 3 presents SEM micrographs of deposited ZnO film sintered at 500 °C and 600 °C at 40 000× magnification. SEM images reveal polycrystalline, smooth, porous and interconnected grains morphology. The small crystallites agglomerates to form spindle, dumbbell, cuboidal shaped particles and fused clusters on surface morphology of this film. As, the sintering temperature increases, the grain size increases due to agglomeration of particles as reflected in 600 °C sintered sample SEM image Figure 3b. At higher temperatures, crystallinity improves with the increase in mobility of atoms at the surface of films. Hence, such types of films may provide novel platform for photovoltaic, sensor and other device applications.

Table 1. Structural, optical and electrical parameters of nanocrystalline ZnO films sintered at different temperatures

Temp °C	$h\ k\ l$	2θ (± 0.001)°	FWHM (± 0.001)°	d (nm)	D (nm)	E_0 (eV)	E_a (eV)
500 °C	1 0 1	37.234	0.2800	2.4734	31	3.21	0.64
600 °C	1 0 1	37.232	0.2600	2.4721	34	3.12	0.61

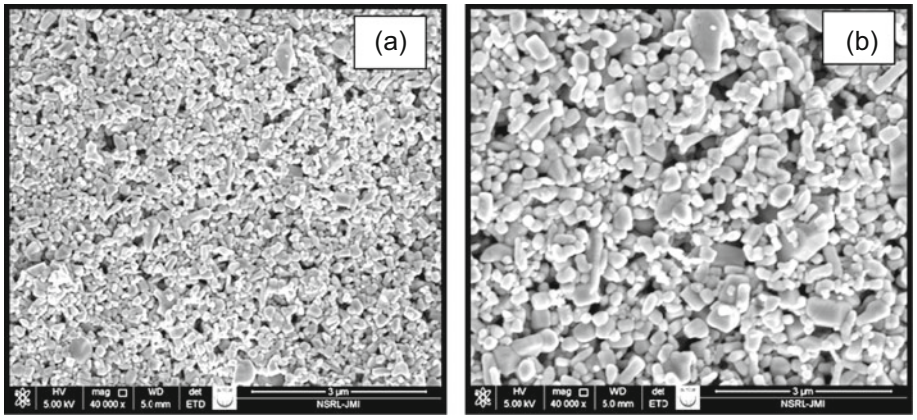

Fig. 3. SEM micrographs of ZnO films sintered at (a) 500 °C and (b) 600 °C temperatures.

3.3 Raman spectroscopy

Raman spectroscopy technique has been used to study vibrational, rotational, and other low-frequency phases in a Raman active compound. ZnO wurtzite structure belongs to C_{6v}^4 space group with two formula units per primitive cell, where all atoms occupy C_{3v} sites. The Raman active optical phonons predicted by the group theory are $A_1 + 2B_1 + 2E_2 + E_1$ where B_1 are silent modes. The phonons of A_1 and E_1 symmetry are polar phonons and, hence, exhibit different frequencies for the transverse-optical (TO) and longitudinal-optical (LO) phonons. Nonpolar phonon modes with symmetry E_2 have two frequencies, E_2 (high) is associated with oxygen atoms vibration and E_2 (low) is associated with Zn sublattice vibrational modes. The E_2 (high) Raman peak exhibits a asymmetrical Lorentzian line shape, red shift and broadens as temperature increases. In Figure 4, Raman spectra of screen printed ZnO thick film sintered at 500 °C and 600 °C temperatures in 1600–200 cm^{-1} region are presented.

The intensity of E_2 (high) mode in both spectra are more as compared to the Raman spectrum of bulk ZnO [27]. The peak at 429 cm^{-1} is assigned E_2 (high) is a symbol of wurtzite phase of ZnO and shows increasing of crystallinity with the increase in sintering temperature. The surface phonon modes in wurtzite nanocrystals appear at frequencies intermediate between A_1 (LO) and E_1 (TO), and the corresponding observed modes in bulk ZnO are obtained at 579 and 413 cm^{-1}, respectively [28]. In the present work, the mode is observed as a very week intensity peak component at 572 cm^{-1} due to breaking of the translation symmetry and localization near the boundary of the crystallites [29]. While the 1144 cm^{-1} is $2A_1$ phonon overtone mode which shifts to 1147 cm^{-1} with

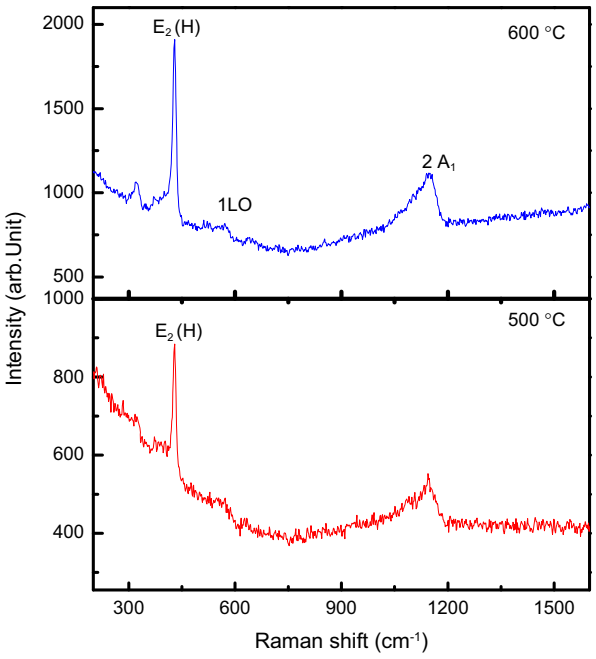

Fig. 4. Raman spectrum of ZnO films sintered at different temperatures.

improvement in intensity. The characteristics of Raman spectra are in good agreement with the XRD results.

3.4 FTIR spectroscopy

FTIR spectroscopy a very important tool has been used for investigating the structural details of bonding groups through their fundamental vibrations available in a

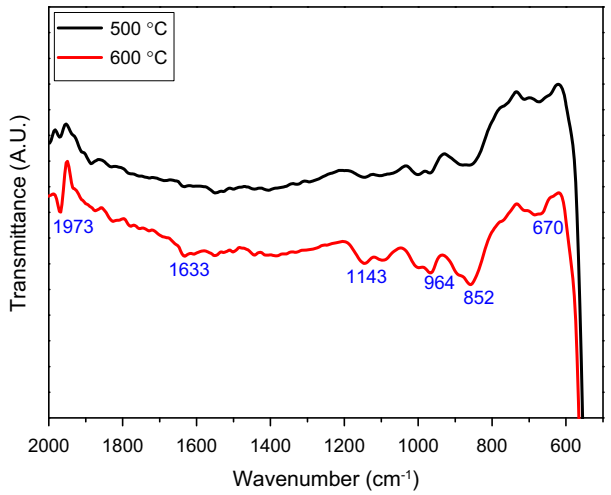

Fig. 5. IR transmission spectrum of ZnO films sintered at different temperatures.

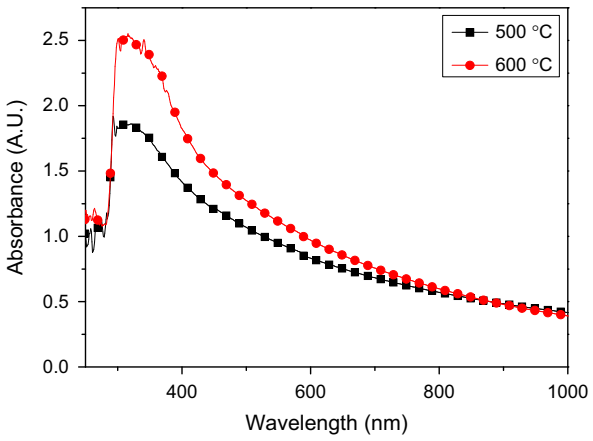

Fig. 6. Absorption spectra of ZnO films sintered at different temperatures.

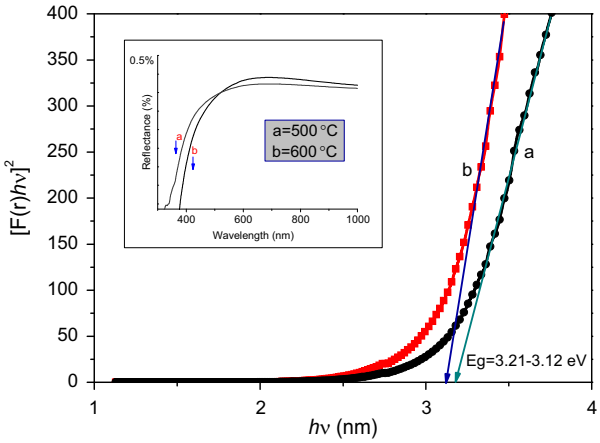

Fig. 7. Energy band gap determination of ZnO films sintered at different temperatures with diffused reflectance spectra inset.

compound. It provides information about functional groups, molecular geometry and inter/intra molecular interactions [30]. IR transmittance spectrum of ZnO film was recorded in the range of 2000–500 cm^{-1} as shown in Figure 5.

Metal oxides generally give absorption bands in fingerprint region i.e., below 1000 cm^{-1} arising from interatomic vibrations. The band positions and absorption peaks not only depend on chemical composition of the film but also depend on the morphology of the film. The transmission bands at 964, 852 are Zn-OH in-plane and out-of-plane bending modes while 670 cm^{-1} mode is attributed to Zn-O stretching vibration [31]. The 1143 cm^{-1} is attributed to Zn-OH stretching and the appearance of this peak shows the adsorption of water in the film from atmospheric moisture and hygroscopic nature of $ZnCl_2$ precursor [32]. 1633 cm^{-1} peak were assigned to water bending mode and 1973 cm^{-1} which arises from the absorption of atmospheric CO_2 on the metallic cations. Similar features have been observed for other the sample. However a slight shift and sharp peaks has been observed with increase in temperature. The shift in band position can be related to the change in the bond length that takes place upon with increase in temperature.

3.5 Optical properties

The UV-visible absorption spectra were recorded in the 250–1000 nm range (Fig. 6). The absorption peak arises from the excitation of electron valence band to conduction band and used to determine the nature and value of optical band gap.

In these spectra, the red shift is observed with increase in sintering temperature i.e., shift to the higher wavelength side. The relation between absorption coefficient (α) and incident photon energy ($h\nu$) can be written as [33]:

$$\alpha h\nu = A(h\nu - E_g)^n, \tag{2}$$

where A is constant, E_g is the energy separation between valence and conduction bands. The optical band gap of the film is obtained by extrapolation of the linear portion of the graph between the modified Kubelka-Munk function $[F(R)h\nu]^2$ versus photon energy ($h\nu$), given by the following relation [34]:

$$F(R) = \frac{(1-R)^2}{2R}, \tag{3}$$

where R is the magnitude of the reflectance as function of energy. The direct band gap comes out to be 3.21 to 3.12 eV according to [35] and is shown in Figure 7 along with inset of diffused reflectance spectra.

This equation is usually applicable for the materials which have high light scattering and absorbing particles in their matrix. Therefore, diffused reflectance is effective for determining the band gap of the solar cell absorbers.

3.6 Electrical conductivity

Electrical conductivity measurement is very important parameter for understanding the nature and type of

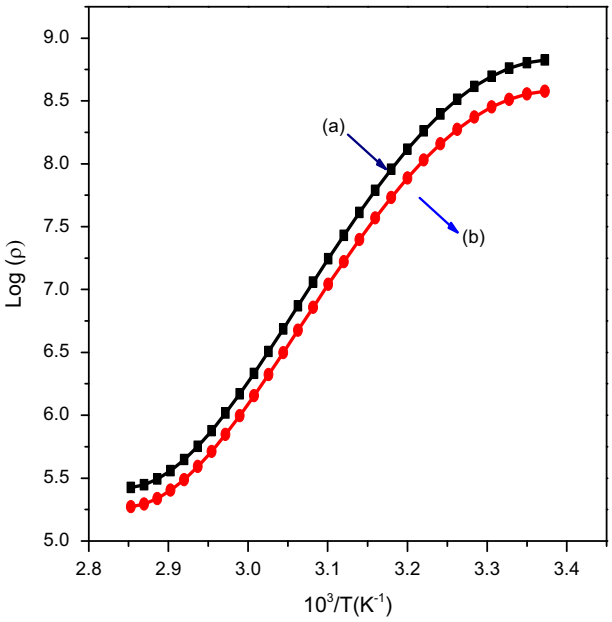

Fig. 8. DC resistivity of ZnO films sintered at (a) 500 °C and (b) 600 °C temperatures.

material for using them electronic device development. Oxides used for thick films can be broadly classified into two groups: metallic, where the resistivity obeys a power-law depending on temperature $\rho \propto T^n$, where $n > 0$; and for semiconducting where resistivity usually follows the exponential law $\rho \propto \exp(\frac{E}{KT})$. The DC electrical conductivity measurements have been carried out in the temperature range 300–400 K. The electrical resistivity (ρ) has been calculated by using the equation (4) [36]:

$$\rho = \frac{\pi t}{\ln 2}\left(\frac{V}{I}\right), \tag{4}$$

ρ is the resistivity (Ω cm), t is the sample thickness (cm), V is the applied voltage and I is the source current (A). The temperature dependency of the DC resistivity can be shown by the well-known Arrhenius equation, given by:

$$\rho = \rho_0 \exp\left(\frac{-\Delta E}{KT}\right), \tag{5}$$

where ρ_0 is the pre-exponential factor, ΔE is the activation energy, K is the Boltzmann constant and T is the temperature (in kelvin). The variation of electrical resistivity with temperature for ZnO is shown in Figure 8.

These plots indicate the semiconducting nature of the samples because resistivity decreases with increase in operating temperature, thus indicating the negative temperature coefficient of resistance. This may be due to the oxygen deficiency of material in it. When we plot the variation between $\log \rho$ and $10^3/\mathrm{T}$, we get activation energy from the slope of the graph that comes out to be 0.64 to 0.61 eV which is in good agreement with the earlier result [37]. The various structural, optical and electrical parameters these ZnO screen printed films sintered at 500 °C and 600 °C are listed in Table 1.

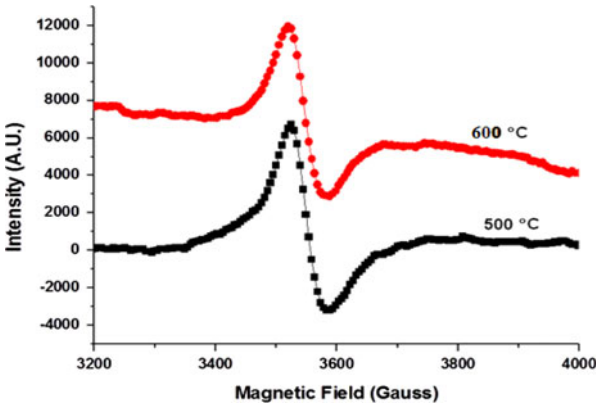

Fig. 9. EPR spectra of ZnO films sintered at different temperatures.

3.7 EPR spectroscopy

EPR spectroscopy has been used to characterize oxygen vacancies in ZnO thick films prepared by screen printing process and sintered at 500 °C and 600 °C temperatures. EPR spectra of the films scratched 1 mg powder recorded at ambient temperature as shown in Figure 9 has Lorentzian shaped resonance signal. The derivative signals have g-values $\sim$ 1.9964 in both the films powder. This signal corresponds to singly ionized oxygen vacancies present in ZnO lattice [38,39] which are formed in these films during growth process when oxidation of zinc takes place by the atmospheric air during sintering process. As the g-value is less than free electron g-value of 2.0023 which indicates the donor origin of the paramagnetic centre. The unstable neutral oxygen vacancies are formed which are easily decomposed to singly ionized oxygen vacancy with single electron. The concentration of oxygen vacancies was calculated by the comparison method using DPPH as standard reference material.

It was found to be 2.3682×10^{18} spin/g and 1.8754×10^{18} spins/g for 500 °C and 600 °C sintered ZnO thick films respectively which is two to three order of higher magnitude than ZnO single crystal. The higher concentration of oxygen vacancies causes narrowing of the energy band gap i.e., from 3.34 eV to 3.21 or 3.12 eV direct energy band gap [40]. The decrease in spin concentration on increasing sintering temperature is attributed to the reduction of defects and ordering of lattice structure by the filling up of the oxygen vacancies.

4 Conclusion

XRD and SEM analysis confirmed the formation of ZnO and the systematic increase in grain size with increase in sintering temperature. IR and Raman spectra showed the vibrational peaks pertaining to hexagonal wurtzite structure of the films. UV-VIS optical studies have been used to calculate direct energy band gap 3.21 to 3.12 eV. The dark DC resistivity reveals the semiconducting nature of films and gives activation energy value in 0.64 to 61 eV range,

hence this exhibits that the conduction process of charge carriers is thermally activated. EPR spectra gives resonance signal pertaining to oxygen vacancies. The higher concentration of oxygen vacancies in these films is also one of the reason in reduction of band gap energy as compared to ZnO single crystal. The concentration of oxygen vacancies decreases with the rise in sintering temperature due to ordering and filling of oxygen vacancies in zinc oxide lattice at higher temperature. Thus, the cost effective and user friendly screen printing technique can be successfully used to fabricate polycrystalline ZnO films having good stability with significant activation energy value. These films are suitable for solar cells and other optoelectronics devices.

The author R.A. Zargar is very thankful to Material Science Research group at CSIR-NPL, New-Delhi for providing the characterization support to pursue this small piece of work.

References

1. S.K. Shukla, E.S. Agorku, H. Mittal, A.K. Mishra, Chemical Papers **68**, 217 (2014)
2. M.M. Hassan, W. Khan, A.H. Azam, J. Lumin. **145**, 160 (2014)
3. H. Wang, J. Xie, K. Yan, M. Duan, J. Mater. Sci. Technol. **27**, 153 (2011)
4. L. Xu, Y.-L. Hu, C. Pelligra, C.-H. Chen, L. Jin, H. Huang, S. Sithambaram, M. Aindow, R. Joesten, S.L. Suib, Chem. Mater. **21**, 2875 (2009)
5. Y. Tong, Y. Liu, L. Dong, D. Zhao, J. Zhang, Y. Lu, D. Shen, X. Fan, J. Phys. Chem. B **110**, 20263 (2006)
6. X. Li, F. Zhang, C. Ma, Y. Deng, Z. Wang, S. Elingarami, N. He, J. Nanosci. Nanotechnol. **12**, 2028 (2012)
7. S. Das, S. Ghosh, Dalton Trans. **42**, 1645 (2013)
8. J. Elias, R. Tena-Zaer, C. Levy-Clement, Thin Solid Films **515**, 8553 (2007)
9. N.H. Al-Hardan, M.J. Abdullah, A.A. Aziz, H. Ahmad, L.Y. Low, Vacuum **5**, 101 (2010)
10. S.K. Kansal, M. Singh, D. Sud, J. Hazard. Mater. **153**, 412 (2008)
11. M. Singhai, V. Chhabra, P. Kang, D.O. Shah, Mater. Res. Bull. **32**, 239 (1997)
12. S. Mondal, P. Mitra, Bull. Mater. Sci. **35**, 751 (2012)
13. X.L. Cheng, H. Zhao, L.H. Huo, S. Gao, J.G. Zhao, Sens. Actuators B **102**, 248 (2004)
14. Y.J. Xing, Z.H. Xi, Z.Q. Xue, X.D. Zhang, J.H. Song, Y.J. Xing, Z.H. Xi, Z.Q. Xue, X.D. Zhang, J.H. Song, Appl. Phys. Lett. **83**, 1689 (2003)
15. A. Khan, M.E. Kordesch, Mater. Lett. **62**, 230 (2008)
16. C.F. Windisch Jr., G.J. Exarhos, C. Yao, L.-Q. Wang, J. Appl. Phys. **101**, 1123711 (2007)
17. J.S. Huang, C.F. Lin, J. Appl. Phys. **103**, 014304 (2008)
18. P. Mitra, A.P. Chatterjee, H.S. Maiti, Mater. Lett. **35**, 33 (1998)
19. R.A. Zargar, S.D. Khan, M.S. Khan, M. Arora, A.K. Hafiz, Phys. Res. Int. **2014**, 464809 (2014)
20. M. Hussain, B.P. Singh, S. Kumar, T.P. Sharma, P.J. Sebastian, Sol. Energy Mater. Sol. Cells **76**, 399 (2003)
21. N. Daneshvar, S. Aber, D. Syed, M.S. Dorajji, A.R. Khataee, M.H. Rasoulifard, Int. J. Chem. Bio. Eng. **1**, 24 (2008)
22. B. Ismail, M. Abaab, B. Rezig, Thin Solid Films **383**, 92 (2001)
23. V. Kumar, M.K. Sharma, T.P. Sharma, Eur. Phys. J. Appl. Phys. **50**, 20502 (2010)
24. S.E. Shaheen, R. Radspinner, N. Peyghambarian, G.E. Jabbour, Appl. Phys. Lett. **79**, 2996 (2001)
25. B.D. Cullity, *Elements of X-ray Diffractions* (Addison-Wesley, Reading, MA, 1978)
26. D. Raoufi, T. Raoufi, Appl. Surf. Sci. **255**, 5812 (2009)
27. H.Z. Wu, K.M. He, D.J. Qiu, D.M. Huang, J. Cryst. Growth **217**, 131 (2000)
28. V.A. Fonoberov, A.A. Baladin, Phys. Rev. B **70**, 233205 (2004)
29. B. Jusserand, M. Cardona, in *Light Scattering in Solids V*, Topics in Applied Physics, edited by M. Carodana, G. Guntherodt, vol. 66 (Springer, Berlin, 1989), p. 49
30. S.K. Nandi, S. Chakraborty, M.K. Bera, C.K. Maiti, Bull. Mater. Sci. **30**, 247 (2007)
31. K. Elen, A. Kelchtermans, H. Van den Rul, R. Peeters, J. Mullens, A. Hardy, M.K. Van Bael, J. Nanomater. **2011**, 390621 (2011)
32. S. Muthukumara, R. Gopalakrishnan, Opt. Mater. **34**, 1946 (2012)
33. J. Tauc (ed.), *Amorphous and Liquid Semiconductors* (Plenum Press, New York, 1974), p. 159
34. S. Cimitan, S. Albonetti, L. Forni, F. Peri, D. Lazzari, J. Colloid Interface Sci. **329**, 73 (2009)
35. A.E. Morales, E.S. Mora, U. Pal, Rev. Mex. Fis. **53**, 18 (2007)
36. Four-point probe manual, EECS143, Micro fabrication Technology
37. Y.H. Kim, H. Kawamura, M. Nawata, J. Mater. Sci. **32**, 1665 (1997)
38. C. Drouilly, J.-M. Krafft, F. Averseng, S. Casale, D.B. Bachi, C. Chizallet, V. Lecocq, H. Vezin, H.L. Pernot, G. Costentin, J. Phys. Chem. C **116**, 21297 (2012)
39. X.J. Wang, L.S. Vlasenko, S.J. Pearton, W.M. Chen, I.A. Buyanova, J. Phys. D: Appl. Phys. **42**, 175411 (2009)
40. J. Wang, Z. Wang, B. Huang, Y. Ma, Y. Liu, X. Qin, X. Zhang, Y. Dai, ACS Appl. Mater. Int. **4**, 4024 (2012)